Chinese Chemical Letters 33 (2022) 2590–2594

Contents lists available at ScienceDirect

Chinese Chemical Letters

journal homepage: www.elsevier.com/locate/cclet

# NiCe bimetallic nanoparticles embedded in hexagonal mesoporous silica (HMS) for reverse water gas shift reaction

Hui Dai[a,b,*], Siqi Xiong[a], Yongqing Zhu[a], Jian Zheng[b], Lihong Huang[a], Changjian Zhou[c,*], Jie Deng[d], Xinfeng Zhang[a]

[a] College of Materials and Chemistry & Chemical Engineering, Chengdu University of Technology, Chengdu 610059, China
[b] Department of Chemical Engineering, Sichuan University, Chengdu 610065, China
[c] School of Chemistry and Chemical Engineering, Yancheng Institute of Technology, Yancheng 224051, China
[d] College of Pharmacy and Bioengineering, Chengdu University, Chengdu 610106, China

ARTICLE INFO

*Article history:*
Received 9 August 2021
Revised 30 August 2021
Accepted 31 August 2021
Available online 6 September 2021

*Keywords:*
Greenhouse gases
Reverse water gas shift reaction
CO selectivity
$CeO_2$
Hexagonal mesoporous silica

ABSTRACT

Reverse water gas shift (RWGS) reaction is a crucial process in $CO_2$ utilization. Herein, Ni- and NiCe-containing hexagonal mesoporous silica (Ni-HMS and NiCe-HMS) catalysts were synthesized using an *in-situ* one-pot method and applied for RWGS reaction. At certain reaction temperatures 500-750 °C, Ni-HMS samples displayed a higher selectivity to the preferable CO than that of conventionally impregnated Ni/HMS catalyst. This could be originated from the smaller NiO nanoparticles over Ni-HMS catalyst. NiCe-HMS exhibited higher activity compared to Ni-HMS. The catalysts were characterized by means of TEM, XPS, XRD, $H_2$-TPR, $CO_2$-TPD, EPR and $N_2$ adsorption-desortion technology. It was found that introduction of Ce created high concentration of oxygen vacancies, served as the active site for activating $CO_2$. Also, this work analyzed the effect of the $H_2/CO_2$ molar ratio on the best NiCe-HMS. When reaction gas $H_2/CO_2$ molar ratio was 4 significantly decreased the selectivity to CO at low temperature, but triggered a higher $CO_2$ conversion which is close to the equilibrium.



Since 1950, the concentration of $CO_2$ attributed to human activities has risen by 30% [1]. $CO_2$ emissions directly cause global warming, projecting the global average temperatures to rise by about 1.5-4.5 °C by 2050 if left unchecked. Moreover, the burning of fossil fuels and excessive deforestation trigger global warming. The capture, utilization, and transformation of $CO_2$ into other energy sources is a potential approach to addressing the menace. The improvement of chemical processes aimed at reducing $CO_2$ emission is a highly effective strategy. In the past year, many countries have unanimously declared that their economies will be carbon-neutral. The $CO_2$ transformation to other energy sources reduces $CO_2$ emissions and alleviates energy shortages [2].

$CO_2$ is a thermodynamically and kinetically stable molecule, making it harder to lose electrons and form $CO_2^+$, while easier to accept electrons and convert C=O bond into C–O bond. Therefore, addition reactions are more likely to occur [3]. For instance, $H_2$ reacts with $CO_2$ to form hydrocarbons, *i.e.*, $CO_2$ hydrogenation reduction. One useful reaction is reverse water gas shift (RWGS), which produces CO, a main C1 chemical raw material that can be converted into other high-value products [4]. Meanwhile, this process is accompanied by other side reactions, including over hydrogenation to generate methane [5,6]. RWGS is a major factor influencing CO selectivity in RWGS reaction, where the activation of $CO_2$ requires significant energy. RWGS reaction is typically processed at high temperature (*e.g.*, > 500 °C), requiring high thermal stability of the used catalyst. For this reaction, noble metals including Pt [7], Pd [8], Rh [9] and Au [10] were applied as catalytic active sites and exhibited excellent performance. Nonetheless, these metals are found in relatively low quantities on earth and at relatively high prices, making them difficult for industrial use. Therefore, research and development of non-precious metals including Cu [11–13] and Ni [14–17] are essential. In recent years, RWGS reactions have widely used Cu-based catalysts, as a substitute for noble metal catalysts. Supported Cu catalysts suffered from low stability in this reaction. For example, the surface area of $Cu/SiO_2$ was significantly reduced after a long-time reaction due to the sintering of the activity components [18]. In contrast with single metal Cu, Ni exhibits better thermal stability for long-term reaction [19–21]. Nevertheless, Ni faces the drawbacks of coke deposition and deactivation. Lu *et al.* [22] observed different forms of NiO particles for the NiO/SBA-15 catalysts, only separated single NiO particles im-

* Corresponding authors.
*E-mail addresses:* daihui18@cdut.edu.cn (H. Dai), zcj@ycit.cn (C. Zhou).

https://doi.org/10.1016/j.cclet.2021.08.129
1001-8417/

proved CO selectivity. Methanation seemingly occurs in aggregated NiO species at lower reaction temperature. Therefore, highly dispersed active Ni particles promotes higher CO selectivity.

Rare earth metal oxide $CeO_2$ as a promoter regulates many reactions due to its redox properties. In the case of dry reforming of methane reaction, the metal support interaction between NiO and ZSM-5 is enhanced by adding Ce as a promoter, which has positive to the catalytic activity [23]. Catalysts prepared with different morphologies of $CeO_2$ as support loaded with Cu have been applied for RWGS, where the amount of surface oxygen vacancies and $Cu^0$ after reduction by $H_2$ increased. The rate of catalytic reaction corresponded with the amount of surface oxygen vacancies for $CeO_2$, participating in $CO_2$ adsorption and activation [24]. The insertion of transition metal like Ni into $CeO_2$ lattice to form Ce–O–Ni solid solution prevents the production of byproduct $CH_4$ [25], however, bulk phase NiO existing in Ni/$CeO_2$ is the active center for synthesis of $CH_4$ [26]. Therefore, the high dispersion of Ni nanoparticles causes higher selectivity of CO [27].

$SiO_2$ mesoporous materials like MCM-41, SBA-15 and hexagonal mesoporous silica (HMS) have drawn significant attention due to their merits including large specific surface area, uniform pore size, and excellent stability, and have been widely used as support in catalysts [28–30]. Among them, HMS with wormhole framework structure incorporates metal into its thick framework wall through neutral amine surfactant and inorganic precursors [31], which is beneficial for the diffusivity of chemical species. Moreover, HMS demonstrated a better thermal stability compared to MCM-41 and SBA-15 [32], also, metals can be uniformly embedded in the HMS skeleton [33–36]. Wang *et al*. synthesized Ni-HMS catalyst using an *in-situ* one-step process, which could perform long-term test at 700 °C in dry reforming of methane for 100 h without significant reduction due to the high dispersion of Ni active sites on support [37]. Sn-HMS catalyst was prepared by a similar method for propane dehydrogenation reaction and remained stable for 170 h after three times of regeneration [38].

This study introduced a timesaving, easy-handling, and energy-saving method for the preparation and characterization of nickel-based catalysts and for the first time, described its application in RWGS reaction. The Ni-HMS and NiCe-HMS were prepared using HMS as support to investigate the influence of reaction temperature from 500 °C to 750 °C for their catalytic performance in RWGS reaction. Further, a series of catalyst characterizations were conducted to better understand the structure and composition of the catalysts as well as explain their catalytic activity. We purposed to prepare a type of RWGS catalyst with effective CO selectivity and better stability using a simple and easy operation method.

The pore structures of three catalysts were investigated by $N_2$ adsorption-desorption at 77 K (Fig. S1a in Supporting information). For Ni-HMS and Ni/HMS samples, a relative pressure range of 0.3–0.5 suggested a Type IV isotherm [39]. For Ni-HMS, the hysteresis loops illustrated that it primarily has a 1D cylindrical channel of uniform mesoporous [37]. Nevertheless, after adding Ce into the HMS structure, the hysteresis loop area was reduced and no clear vertical asymptote displayed a Type Iisotherm, which could be attributed to the certain pores of the were loaded by Ce species [40]. Combined with pore size distribution curves (Fig. S1b in Supporting information), the pore diameter was concentrated between 2–5 nm on mesoporous. Among the three catalysts, the Ni/HMS exhibited the largest surface area 782 $m^2/g$, pore-volume 0.87 $cm^3/g$, and diameter 3.5 nm. These physical data were reduced when Ni or Ce nanoparticles were embedded into the structure of HMS, due to the fact that the incorporation of Ni and Ce into the HMS framework occupied a part of the surface structure.

TEM characterization was conducted on the samples to analyze the nanoparticle distribution of catalysts from the microstructure. The results are shown in Fig. 1. HMS supported presents the

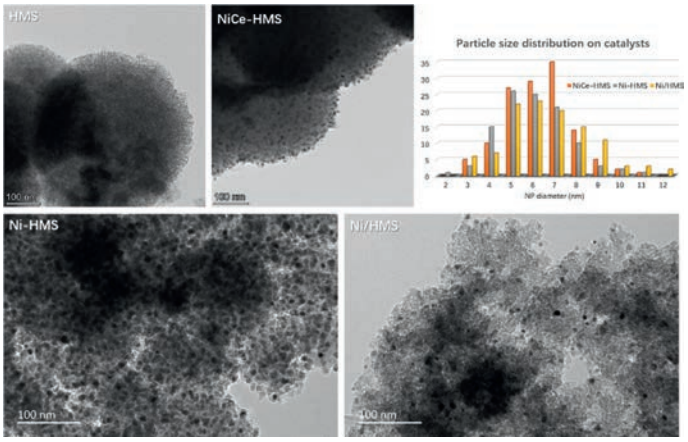


**Fig. 1.** TEM images and nickel particle size distribution of the samples.

**Table 1**
Physicochemical properties of the catalysts

| Samples | $S_{BET}$ ($m^2/g$) [a] | $V$ ($cm^3/g$) [a] | $d$ (nm) [a] | Ni loading (wt%) [b] |
|---|---|---|---|---|
| NiCe-HMS | 389 | 0.24 | 2.5 | 4.43 |
| Ni-HMS | 414 | 0.32 | 2.7 | 4.41 |
| Ni/HMS | 782 | 0.87 | 3.5 | 3.30 |

[a] Measured using $N_2$ adsorption-desorption.
[b] Measured using ICP-OES.

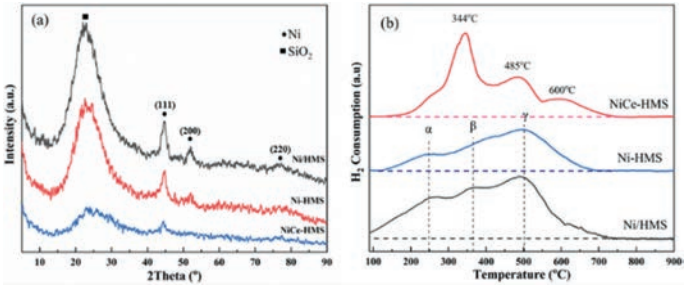


**Fig. 2.** XRD partten (a) for the reduced catalysts and $H_2$-TPR (b) profiles of the fresh catalysts.

wormhole-like framework. Ni-HMS and NiCe-HMS catalysts show the metal oxide particles ordered insert into the hexagonal framework. For Ni/HMS catalyst, the NiO particles were distributed on the surface of HMS by counting the diameter of NiO particles ranging between 3 nm and 12 nm. Combined with the actual content of Ni tested by ICP-OES shown in Table 1, Ni/HMS the content was low while the grain was large. This accounts for the most of NiO particles distributed out of the pore. The average particle size of the three catalysts ranged from large to small, *i.e.*, Ni/HMS (7.1 ± 0.2 nm) > NiCe-HMS (6.7 ± 0.2 nm) > Ni-HMS (6.5 ± 0.2 nm). Ni/HMS unlike the other two had a weak metal-support interaction. As for NiCe-HMS, NiO and $CeO_2$ nanoparticles co-existed on support, while the average particle size was calculated by all the particles. EDX mapping analysis was used to confirm the successful addition of Ce into NiCe-HMS catalyst (Fig. S2 in Supporting information). In NiCe-HMS, Ni and Ce were highly dispersed on the carrier HMS, suggesting that the introduction of Ce enhanced the dispersion of Ni and thus showed a significant structural advantage.

Characterization of the catalyst were performed by XRD (Fig. 2a), and the typical peak at 22.9° was associated with supported HMS crystalline phase (JCPDS No. 49-0623), which exists in

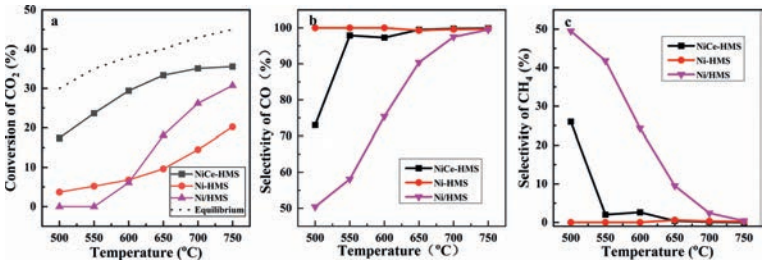


**Fig. 3.** Catalytic activity of three catalysts applied to RWGS: (a) $CO_2$ conversion; (b) CO selectivity; (c) $CH_4$ selectivity.

three catalysts. In addition, others three peaks were belong to the (111), (200) and (220) crystal face of metal Ni, respectively (JCPDS No. 04-0850) [41]. For Ni-HMS and Ni/HMS, these peaks are relatively sharp, indicating that Ni species are relatively non-uniform and exhibit as larger particles. Combined with the actual content of Ni tested by ICP-OES showed in Table 1, the sharpest diffraction peak of Ni/HMS was found to have the smallest Ni loading of 3.3 wt%, illustrating that Ni nanoparticles are not well dispersed into the supported channel. The peak intensity of Ni-HMS with higher Ni content was obviously lower, indicating that the different preparation methods would directly influence dispersion of the active species. In contrast, NiCe-HMS had the highest loading of 4.43 wt%, while the diffraction peak was not obvious. Only Ni diffraction peak and no diffraction peak ascribed to the Ce metal was found, implying that Ce might increase the dispersion of Ni nanoparticles. All of the above results provide a good support for TEM observation.

$H_2$-TPR test was used to explore the interaction between metal oxides and support (Fig. 2b). By comparing all the three samples, the peak area of Ni/HMS was the highest. Combined with the previous analysis, the metal nanoparticles of the other two catalysts were partially embedded into the wall of support, causing a reduction of only a fraction of metal oxides. The reduction peaks of Ni-HMS and Ni/HMS exhibited similar temperature ranges, but different peak areas. The peak centered around 250 °C and 350 °C attributed the reduced surface of isolated bulk NiO particles and weak interacted with support, defined as $\alpha$, $\beta$, respectively[41]. The higher reduction peak range was represented as $\gamma$, ascribed to the reduction of NiO on the wall subsurface[37]. In contrast with Ni-HMS and NiCe-HMS, the reduction temperature of Ni/HMS was relatively lower and intensity was relatively higher, deducing that the preparation method affects the interaction between the Ni and carrier [42]. For NiCe-HMS catalyst, reduced peak at 344 °C peak sharpness, attributed to NiO in close contact with $CeO_2$ and the chemisorbed oxygen in the oxygen vacancies of $CeO_2$ [43]. 500 °C-600 °C had the wide and lower intense reduction peaks, which belong to the simultaneous reduction of $NiO_x$ and surface $CeO_2$ [44]. These two types of species were also the active sites of $CO_2$. The high reduced temperature was ascribed to the reduction of metal particles embedded in mesoporous carriers [45]. Therefore, the *in-situ* preparation method enhances the interaction between the active phase and support. The addition of Ce maintains the dispersibility of active metals, with lots of NiO distributed close to $CeO_2$ existing in the interface between Ni-Ce.

All the catalysts were applied in the RWGS reaction at the temperature range of between 500 °C and 750 °C. Fig. 3 shows the conversion of $CO_2$, selectivity of CO and $CH_4$ as a function of reaction temperature. Unlike NiCe-HMS, other catalysts revealed relatively poor catalytic performance in $CO_2$ conversion. Chen *et al.* [46], noted that the bare $CeO_2$ catalyst participates in $CO_2$ transformation in RWGS reaction, meanwhile they produced CO from the surface oxygen vacancies, causing a satisfactory catalytic performance of NiCe-HMS. Ni-HMS exhibits a $CO_2$ conversion of 3.7% in 500 °C, apparently higher than Ni/HMS. However, with increased temperature, $CO_2$ conversion of Ni/HMS was higher than Ni-HMS, suggesting that Ni/HMS exposed more Ni particles. For Ni-HMS, it had the highest CO selectivity of up to 99.9% among the three catalysts, benefiting from the *in-situ* preparation method that triggers uniform dispersion of Ni nanoparticles. The RWGS reaction was applied as an endothermic reaction, more favorable to enhance CO selectivity with the increase of reaction temperature. All the catalysts reached CO selectivity of 99.3% at approximately 750 °C. In contrast, the CO selectivity of Ni/HMS was low because the bulk Ni particles readily produced $CH_4$ [47]. Conclusively, Ni-based catalyst prepared by the *in-situ* method exhibited a higher CO selectivity than conventional prepared catalyst. Meanwhile, adding Ce increased $CO_2$ conversion. In combination with TPR, higher $CO_2$ conversion was ascribed to the neighboring oxygen vacancies forming the interface of Ni and Ce, active sites for $CO_2$ hydrogenation [48]. A high dispersion of nanoparticles of NiCe-HMS increased the activity oxygen vacancies improving the efficiency in the RWGS reaction [48].

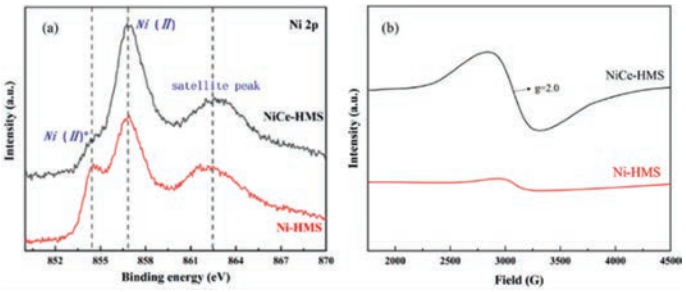


**Fig. 4.** (a) Ni 2p XPS spectra of fresh catalysts NiCe-HMS and Ni-HMS. (b) EPR spectra of reduced catalysts Ni-HMS and NiCe-HMS.

The XPS in Fig. 4a demonstrates the chemical states of Ni 2p for NiCe-HMS and Ni-HMS. Three peaks of Ni species were reported and the two lower binding energy represented different environments of surface Ni species. Binding energy around 854 eV consistent Ni(II)* species represented the bigger NiO particles. Binding energy at 856.9 eV defined as Ni(II), which was the presence of NiO highly dispersed on the support surface, created higher metal-support interaction. The other broad peak was the shakeup satellite peak [49]. Unlike the first two peaks intensity, Ni(II)* for Ni-HMS was significantly more than NiCe-HMS catalyst. Combined with the previous characterization analysis, this result once again confirmed that the doped Ce reduced the particle size of the active component. Meanwhile, it had better metal support interaction compared to the intensity of Ni(II).

EPR test was employed to further confirm the existence of oxygen vacancy. As shown in Fig. 4b, at about g = 2.0, sample NiCe-HMS shows a higher EPR signal than sample Ni-HMS, which is

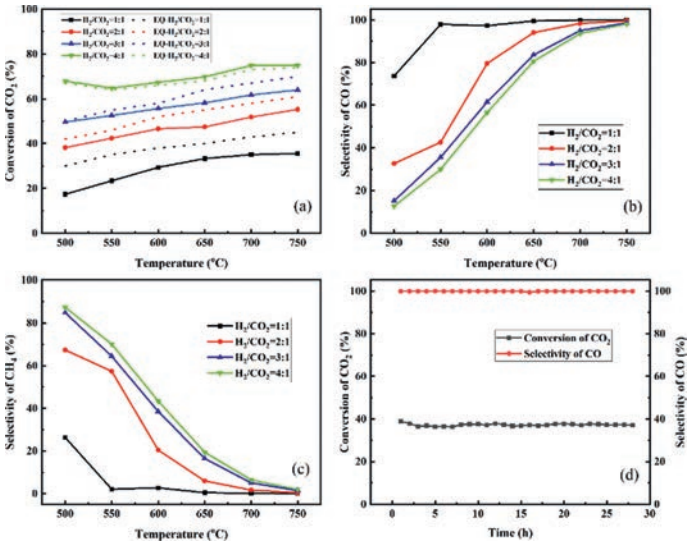


**Fig. 5.** Catalytic activity of catalyst NiCe-HMS applied to RWGS at different inlet ratios: (a) $CO_2$ conversion; (b) CO selectivity; (c) $CH_4$ selectivity; (d) The catalytic activity of NiCe-HMS for 28 h at 750 °C.

a typical signal of oxygen vacancy (OVs) [50]. The existence of oxygen vacancy prevents forming Lewis basic position, which may strongly adsorb and activate gaseous $CO_2$ and enhance the catalytic activity of RWGS. Which results also verified by $CO_2$-TPD (Fig. S3 in Supporting information).

Effect of feed ratio on the catalytic activity, CO selectivity, and $CH_4$ selectivity were investigated on NiCe-HMS at 500–750 °C, and the results are shown in Figs. 5a–c. As shown, with the increase of $H_2/CO_2$ molar ratio from 1 to 4, $CO_2$ conversion increased, while CO selectivity decreased while $CH_4$ selectivity increased, specifically at lower reaction temperature [51], meanwhile, the $CO_2$ conversion was close to equilibrium. Ni demonstrated a better $H_2$ dissociation activity, when the $H_2$ feed ratio increased, a higher $CH_4$ formed specifically in 500 °C [52]. The NiCe-HMS catalyst exhibited a high activity in RWGS with CO yield of up to 35.3% at a ratio of $H_2/CO_2 = 1$, with a ratio of $H_2/CO_2 = 4$ CO yield rising to 74.4% at 700 °C. Therefore, higher CO selectivity fed gas $H_2/CO_2$ of 1, while, higher $CO_2$ conversion preferred the $H_2/CO_2$ of 4. In order to demonstrate the stability of NiCe-HMS catalyst, it was used in reverse water gas shift reaction at 750 °C for 28 h. As shown in Fig. 5d, the stability maintains well, albeit with high activity and stability for a long time. The conversion of $CO_2$ and selectivity of CO maintains stable, which can be attributed to the good thermal stability and resistance to carbon deposition of NiCe-HMS catalyst. Therefore, the NiCe-HMS catalyst may be a promising candidate for industrial application in the future.

In conclusion, NiCe-HMS and Ni-HMS were prepared by one-pot *in-situ* route and applied in RWGS reaction at the temperature range of 500-750 °C. The selectivity to CO on these samples was significantly enhanced compared to conventionally impregnated Ni-HMS. This benefited from the highly dispersed Ni nanoparticles formed on the surface of the support, inhibiting the generation of $CH_4$. In contrast with Ni-HMS, after adding Ce, the conversion of $CO_2$ increased due to the large amount of NiO nanoparticles existing close to $CeO_2$. And a high dispersed Ni and Ce nanoparticles interface formed more active oxygen vacancies and efficient reaction sites for $CO_2$ hydrogenation. The catalysts prepared by the one-pot *in-situ* method outperformed those prepared by the traditional impregnation method. When the ratio of $H_2/CO_2 = 4$, the conversion of $CO_2$ was close to the equilibrium. Our findings provide a promising strategy for the development of a bimetal catalyst system in RWGS.

## Declaration of competing interest

There are no conflicts to declare.

## Acknowledgments

The authors thank to the Chengdu University of Technology Teachers Development Research Fund (No. 10912-2019KYQD07266) and National Natural Science Foundation of China (No. 21806015) for financial support.

## Supplementary materials

Supplementary material associated with this article can be found, in the online version, at doi:10.1016/j.cclet.2021.08.129.

## References

[1] N. Charisiou, G. Siakavelas, L. Tzounis, et al., Int. J. Hydrogen Energy 43 (2018) 18955–18976.
[2] Y.H. Wu, Q. Chen, S. Liu, et al., Chin. Chem. Lett. 30 (2019) 2186–2190.
[3] G. Zhou, B. Dai, H. Xie, et al., J. $CO_2$ Utilization 21 (2017) 292–301.
[4] H. Yang, C. Zhang, P. Gao, et al., Catal. Sci. Technol. 7 (2017) 4580–4598.
[5] Y. Wang, H. Arandiyan, S.A. Bartlett, et al., Appl. Catal. B: Environ. 277 (2020) 119029.
[6] Y.H. Dai, M. Xu, Q.J. Wang, et al., Appl. Catal. B: Environ. 277 (2020) 119271.
[7] S.M. Lee, H. Eom, S.S. Kim, Environ. Technol. 40 (2019) 182–192.
[8] F.C. Meunier, D. Tibiletti, A. Goguet, D. Reid, R. Burch, Appl. Catal. A: Gen. 289 (2005) 104–112.
[9] M. Maestri, K. Reuter, Chem. Eng. Sci. 74 (2012) 296–299.
[10] A.A. Upadhye, I. Ro, X. Zeng, et al., Catal. Sci. Technol. 5 (2015) 2590–2601.
[11] X. Hu, X.S. Hu, Q.X. Guan, et al., Sustain. Energy Fuels 4 (2020) 2937–2949.
[12] C.A. Galvan, J. Schumann, M. Behrens, et al., Appl. Catal. B: Environ. 195 (2016) 104–111.
[13] Q. Zhang, L. Pastor-Perez, W. Jin, et al., Appl. Catal. B: Environ. 244 (2019) 889–898.
[14] J.X. Chen, Q.W. Long, K. Xiao, et al., Sci. Bull. 66 (2021) 1063–1072.
[15] B. Dong, J.Y. Xie, Z. Tong, et al., Chin. J. Catal. 41 (2020) 1782–1789.
[16] L.L. Zeng, L.J. Yang, J. Lu, et al., Chin. Chem. Lett. 29 (2018) 1875–1878.
[17] X.D. Zhang, K. Liu, J.W. Fu, et al., Front. Phys. Beijing 16 (2021) 63500.
[18] C.S. Chen, W.H. Cheng, S.S. Lin, Chem. Commun. (2001) 1770–1771.
[19] A. Ranjbar, A. Irankhah, S.F. Aghamiri, Res. Chem. Int. 45 (2019) 5125–5141.
[20] F.M. Sun, C.F. Yan, Z.D. Wang, C.Q. Guo, S.L. Huang, Int. J. Hydrogen Energy 40 (2015) 15985–15993.
[21] L. Yang, L. Pastor-Perez, S. Gu, A. Sepulveda-Escribano, T.R. Reina, Appl. Catal. B: Environ. 232 (2018) 464–471.
[22] B.W. Lu, K. Kawamoto, RSC Adv. 2 (2012) 6800–6805.
[23] N.B. Gao, M.X. Cheng, C. Quan, Y.P. Zheng, Fuel 273 (2020) 117702.
[24] G.L. Zhou, F.Q. Xie, L.D. Deng, G.Z. Zhang, H.M. Xie, Int. J. Hydrogen Energy 45 (2020) 11380–11393.
[25] B.C. Dai, G.L. Zhou, S.B. Ge, et al., Can. J. Chem. Eng. 95 (2017) 634–642.
[26] L.H. Wang, H. Liu, Y. Liu, Y. Chen, S.Q. Yang, J. Rare Earth 31 (2013) 969–974.
[27] B.W. Lu, K. Kawamoto, Mater. Res. Bull. 53 (2014) 70–78.
[28] V. Parvulescu, C. Dascalescu, B.L. Su, Nanotechnol. Mesostruct. Mater. 146 (2003) 629–632.
[29] R. Wojcieszak, S. Monteverdi, M. Mercy, et al., Appl. Catal. A: Gen. 268 (2004) 241–253.
[30] T. Kang, Y. Park, J. Yi, J. Mol. Catal. A: Chem. 244 (2006) 151–159.
[31] T.R. Pauly, Y. Liu, T.J. Pinnavaia, S.J.L. Billinge, T.P. Rieker, J. Am. Chem. Soc. 121 (1999) 8835–8842.
[32] P.T. Tanev, T.J. Pinnavaia, Chem. Mater. 8 (1996) 2068–2079.
[33] Y.Y. Liu, K. Murata, M. Inaba, N. Mimura, Appl. Catal. A: Gen. 309 (2006) 91–105.
[34] S.S. Bhoware, S. Shylesh, K.R. Kamble, A.P. Singh, J. Mol. Catal. A: Chem. 255 (2006) 123–130.
[35] E. Lira, C.M. Lopez, F. Oropeza, et al., J. Mol. Catal. A: Chem. 281 (2008) 146–153.
[36] I.S. Ke, S.T. Liu, Appl. Catal. A: Gen. 317 (2007) 91–96.
[37] M. Wang, Q. Zhang, T. Zhang, et al., Chem. Engin. J. 313 (2017) 1370–1381.
[38] G.W. Wang, H.L. Zhang, Q.Q. Zhu, et al., J. Catal. 351 (2017) 90–94.
[39] M. Thommes, K. Kaneko, A.V. Neimark, et al., Pure Appl. Chem. 87 (2015) 1051–1069.
[40] D.Y. Zhao, J.L. Feng, Q.S. Huo, et al., Science 279 (1998) 548–552.
[41] J.X. Chen, J.J. Zhou, R.J. Wang, J.Y. Zhang, Ind. Eng. Chem. Res. 48 (2009) 3802–3811.
[42] J.E. Spanier, R.D. Robinson, F. Zheng, S.W. Chan, I.P. Herman, Phys. Rev. B 64 (2001) 245407.

[43] M. Peymani, S.M. Alavi, M. Rezaei, Int. J. Hydrogen Energy 41 (2016) 6316–6325.
[44] C. Alvarez-Galvan, J.L. Martinez, M. Capel-Sanchez, L. Pascual, J.A. Alonso, Adv. Sustain. Syst. (2021) 2100029.
[45] Z.Y. Zakaria, J. Linnekoski, N.A.S. Amin, Chem. Engin. J. 207 (2012) 803–813.
[46] X. Chen, X. Su, B. Liang, et al., J. Energy Chem. 25 (2016) 1051–1057.
[47] G. Zhou, H. Liu, K. Cui, et al., Int. J. Hydrogen Energy 42 (2017) 16108–16117.
[48] Y. Liu, Z. Li, H. Xu, Y. Han, Catal. Commun. 76 (2016) 1–6.
[49] C. Italiano, J. Llorca, L. Pino, et al., Appl. Catal. B: Environ. 264 (2020) 118494.
[50] Y.C. Huang, H.B. Li, M.S. Balogun, et al., ACS Appl. Mater. Int. 6 (2014) 22920–22927.
[51] A. Ranjbar, A. Irankhah, S.F. Aghamiri, J.f Environ. Chem. Engin. 6 (2018) 4945–4952.
[52] S. Choi, B.I. Sang, J. Hong, et al., Sci. Reports 7 (2017) 41207.